Signal Processing and Renewable Energy
March 2021, (pp. 1-14)
ISSN: 2588-7327
eISSN: 2588-7335

Estimation of the Bistatic Echolocation from Underwater Target Using Ship Noise based on Normal-Mode Model

Mojgan Mirzaei Hotkani[1], Seyed Alireza Seyedin[1*], Jean-Francois Bousquet[2]

[1] Department of Electrical Engineering, Ferdowsi University of Mashhad, Mashhad, Iran.
[2] Department of Electrical & Computer Engineering, Dalhousie University, Halifax, NS, Canada.

Received: 23-Oct-2020, Revised: 18-Nov-2020, Accepted: 24-Nov-2020.

Abstract

In this paper, a novel application that uses the broadband noise from a ship-of-opportunity to estimate the scattering from underwater objects is reported. The propagation is based on the normal-mode model. The source localization (location of propeller) is initially realized using incoherent broadband matched-field processing. Then, by utilizing an estimator that relies on Normal-Modes, the target echo below the sea surface is calculated to evaluate the location of the target. The proposed idea is illustrated using simulation and then verified using the acoustic data from a 2019 underwater communication trial in Grand Passage, Nova Scotia in Canada. Experimental results show that the proposed technique can be a reliable signaling method and environmentally friendly that can be applied to the fields of underwater communication and ocean monitoring for a shallow water environment.

Keywords: Bistatic Echolocation, Normal-Mode Model, Matched-Field Processing, Underwater Localization, Ship-Of-Opportunity.

1. INTRODUCTION

Sources of opportunity allude to any source of acoustic energy existing in the maritime environment not generated for the explicit aim of ocean sensing. Wave noise and sea ice are instances of acoustic sources of opportunity that have been used in the past [1].

Recently, a few studies utilized shipping noise as an opportunistic active source to estimate the geoacoustic properties of the seabed by using commercial vessels or small ships [2, 3]. It has been observed that ships

*Corresponding Authors Email: seyedin@um.ac.ir

are powerful and potentially underutilized acoustic sources of opportunity. They can also be operated to obtain information about the marine environment and target localization.

The noise sources that act as broadband signals on ships can be categorized as follows:

- The parts of the driving force generators include the engine, gear, piston movements, and combustion system of the cylinders;
- The spinning propeller;
- Moving accessories including the generator, ventilation system and pumps;
- Hydrodynamic effects.

The noise produced from the spinning propeller is one of the most energetic noises due to the ship movement [4]. The intensity of the generated noise ship depends on the loading on the blades, the flow of the environment, size of the ship, propeller diameter, number of blades, rotational speed, maintenance conditions, and operating speed [5].

The rotation of the blades around the propeller axis causes the cavitation phenomenon. Specifically, cavitation causes a rapid change of pressure in a liquid, which leads to small vapor-filled cavity formations in places where the pressure is relatively low. At higher pressures, these cavities, called "bubbles" or "voids", collapse and can generate an intensive shock wave [6].

Propeller noise can be classified into three categories: harmonic noise, broadband noise, and narrow-band noise. Underwater noise from ships is produced during normal conditions from propeller cavitation, which is known to peak between 50 to 150 Hz but can extend up to 10 kHz [7]. The ranges of underwater noise frequencies that are produced by ships are shown in Fig. 1.

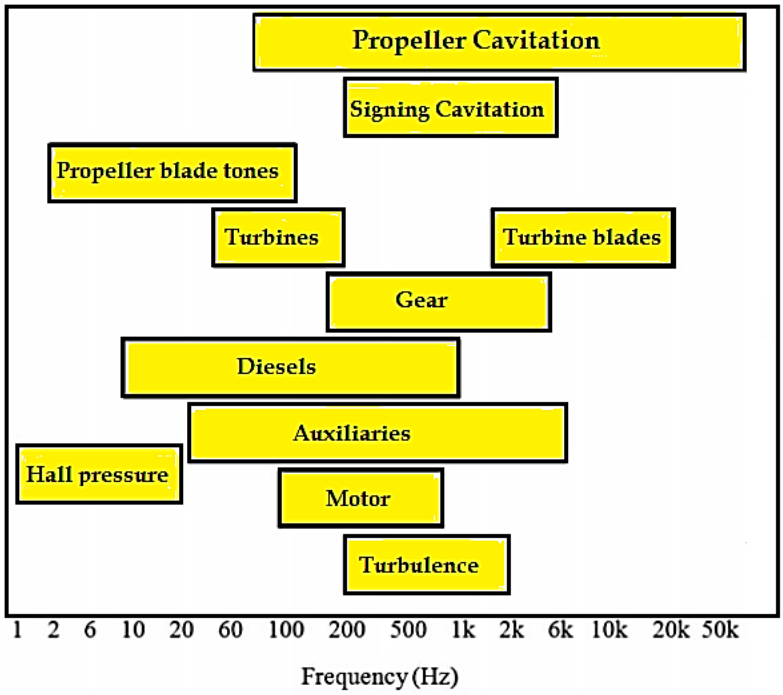

Fig. 1. The frequency ranges of the sources for ship noise [14].

Detecting underwater inanimate objects such as pieces of airplanes dropped in the water or submerged vessels is an important challenge in ocean exploration.

So far, the methods used for solving these problems are based on active sonars.

This paper proposes a new idea that examines the noise propagation ability of a ship's noise as an opportunistic source to identify the location of underwater targets. Specifically, the noise produced by the ship's spinning propellers acts as a source.

As such, the proposed method offers a way to achieve passive localization and avoid the use of a human-made source.

Using ship noise as an exciting signal, underwater localization becomes an environmentally friendly and low-cost technique for ocean monitoring. However, based on our knowledge, the present work is the first application towards underwater target localization using the scattering of ship noise from targets. In our previously published paper [6], we presented this concept for object localization and utilized the Wittekind method to model the noise, and we used multiple signal classification (MUSIC) to find the location of the target in MATLAB and COMSOL.

In this paper, we demonstrate this idea by using realistic data and new localization algorithms.

Sound propagation in water is mathematically modeled using the Helmholtz equation based on the boundary conditions of the underwater environment. Generally, there are five types of models for solving the wave equation, such as the fast field program (FFP), normal modes, ray theory, the parabolic equation (PE), and finite element (FE) solution [8].

The acoustic propagation in shallow water is described accurately using environmental parameters that include sound speed profile, the density of water, and the group velocity of modes. So, it seems to be the best solution for the scattering problem. This idea was first presented by Bucker and Morris [9], and later, it was improved by Zhang and Jin [10]. The measurement of normal-mode reverberation and target echo models for monostatic and bistatic geometries has been presented in [11].

The focus of the present study is to locate the target echo using bistatic geometry and is based on isovelocity and shallow water environment. Indeed, the source localization is firstly performed using matched-field processing (MFP).

MFP is obtained by matching the measured pressure fields at hydrophones with replica pressure fields which are constructed by a wave propagation model according to the supposed source locations and environmental parameters [12].

The rest of this paper is organized as follows: In Section 2, the experimental setup and data collection are investigated. The target echo is defined in Section 3. The proposed technique and simulation results for the synthetic data are presented in Section 4 and Section 5, respectively. Experimental results for the Grand Passage data set are given in Section 6. Finally, the conclusions are presented in Section 7.

2. EXPERIMENTAL SETUP AND DATA COLLECTION

The data analyzed in this paper were produced by a fishing boat and ferry noise that was collected over seven days. The experiment took place on August 14, 2019, in Grand Passage, Nova Scotia, Canada. The equipment deployed during this trial consists of three linear power amplifiers that were also used to evaluate the reliability of acoustic communication, as well as a DC power supply, and a 5-element hydrophone array shown in Fig. 2. A waterproof, pressure-resistant, battery-powered case serves to record and store data from the hydrophone array shown in Fig. 2, and a weighted cage protects the equipment. The plate of hydrophones is installed to be a few cm above the rail of the cage. The array is deployed horizontally at a depth of 19.3 m. The bearing of the array relative to the vessel is shown in Fig. 3.

The distance between any two adjacent corner elements is approximately 0.228 m, also, the distance from any corner element to the center element is approximately 0.165 m. It should be noted that the distance between the two hydrophones was chosen in such a way that aliasing does not occur for the frequencies of interest.

It is also important to note that the ocean conditions in Grand Passage are subject to a very high flow environment with high tides. The exact location and approximate bearing of the boat when the receiver was deployed is shown in Fig. 3. Fig. 4 shows the boat that traveled to known positions near the array during the experiment.

This experiment is designed to support an underwater communication trial and was also defined to test localization in a shallow water environment, in which there is significant scattering from the seafloor and target. Physical parameters of the environment during the tests are summarized as follows:

- Density of water, $\rho = 1000$ kg/m^3.
- Depth of sea: D = 20 m.
- Sound speed: c = 1595 m/s.
- Frequency band of the propeller noise: f = 2-3 kHz.

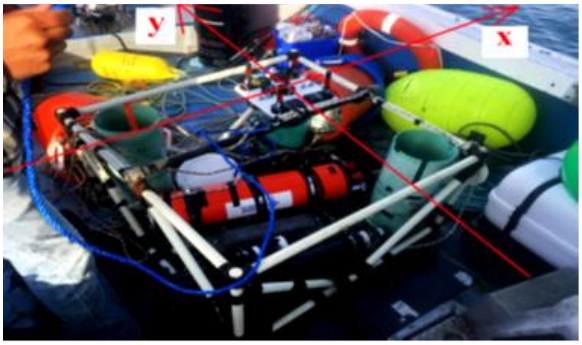

Fig. 2. Experimental setup before being deployed underwater.

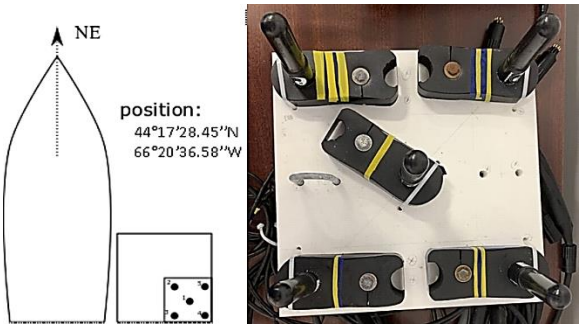

Fig. 3. Location and bearing of the vessel during deployment of the receiver.

Fig. 4. Experiment scenario and the fishing boat in the Bay of Fundy.

3. TARGET ECHO

Generalizing the target echo formulation for the bistatic geometry from Ellis [11] used the normal modes and considered an isovelocity problem (the sound speed profile and density of water are constant) in the shallow water environment, and the total propagation gain is modeled as:

$$P_r(r,z) = (P_{st} \times P_{tr}) + P_{sr} \tag{1}$$

where P_r, P_{st}, P_{tr}, and P_{sr} are the total pressure field at the receiver, the incident acoustic pressure received at the target from the source, the acoustic pressure gain between the target and receiver, and the acoustic pressure gain between the source and receiver, respectively. P_{st}, P_{tr}, and P_{sr} are calculated as:

$$P_{st} = S \times \frac{i}{\rho(z_s) \times \sqrt{8\pi r_{st}}} \times e^{-i\pi/4} \times \sum_{n=1}^{M} (\Psi_n(z_s) \times \Psi_n(z_t) \times \frac{e^{k_{rn} r_{st}}}{\sqrt{k_{rn}}}), \tag{2}$$

$$P_{tr} = T \times \frac{i}{\rho(z_t) \times \sqrt{8\pi r_{tr}}} \times e^{-i\pi/4} \times \sum_{m=1}^{M} (\Psi_m(z_t) \times \Psi_m(z_r) \times \frac{e^{k_{rm} r_{tr}}}{\sqrt{k_{rm}}}), \tag{3}$$

$$P_{sr} = S \times \frac{i}{\rho(z_s) \times \sqrt{8\pi r_{sr}}} \times e^{-i\pi/4} \times \sum_{j=1}^{M} (\Psi_j(z_s) \times \Psi_j(z_r) \times \frac{e^{k_{rj} r_{sr}}}{\sqrt{k_{rj}}}), \tag{4}$$

where $S, z_s, r_{st}, \Psi_n, z_t, M, k_{rn}, k_{zn}, T, r_{tr}, r_{sr}$ and z_r are the source power strength, the depth of source, the horizontal range between the source and target, the modes function, the depth of the target, the maximum number of modes, the horizontal wave-number, the vertical wave-number, the scattering power strength of the target, the horizontal range between the target and receiver, the horizontal range between the source and receiver, and the depth of receiver, respectively. Also, i is the imaginary unit. The maximum number of modes and modes functions are obtained using:

$$\begin{cases} \Psi_n(z) = \sqrt{\frac{2\rho}{D}} \sin(k_{zn} z), \;\; k_{zn} = (n - \frac{1}{2}) \times \frac{\pi}{D} \\ k_{rn} = \sqrt{(\frac{2\pi f}{c})^2 - k_{zn}^2}, \\ M \le \frac{kD}{\pi} = \frac{2 f_{\max} D}{c} \end{cases} \tag{5}$$

where $f_{\max}$ is considered to be the maximum frequency of the signal. The mth mode has m zeroes in the interval [0, D].

Fig. 5 shows the 20th mode for the isovelocity problem with the physical parameters of the Grand Passage environment and considers an average frequency of 2500 Hz.

4. PROPOSED TECHNIQUE

To locate the scatterer, firstly the location of the source must be determined. For this purpose, the proposed algorithm, summarized in Table 1 is developed and tested.

The MFP algorithm is based on the match between the received signal at the hydrophone array and the replica signal and the estimate is obtained by scanning the source position in space to provide an

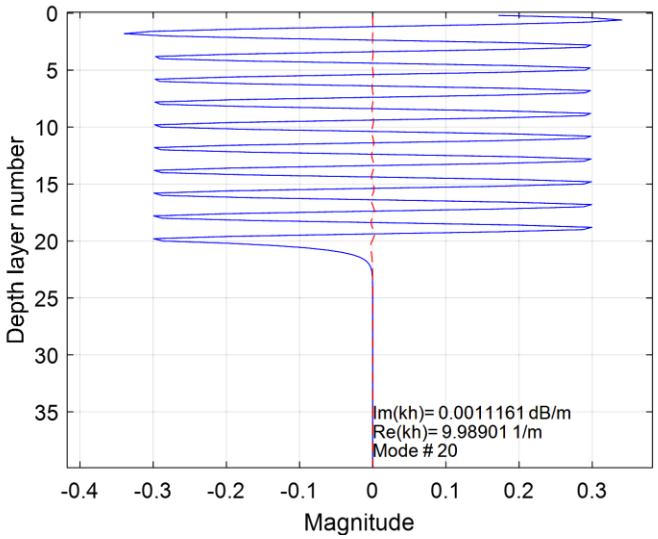

Fig. 5. 20th mode of the isovelocity problem.

estimation of the source location. In the proposed method, the match between the cross-correlation of the model signals and the cross-correlation of the received signals for each frequency has been calculated using the mean squared error. Therefore, the incoherent broadband MFP that estimates the source location in our method, is defined as

$$(\hat{x},\hat{y},\hat{z}) = \arg\max_{x,y.z}\{A(f,x,y,z)\}$$
$$A(f,x,y,z) = \sum_{f}\Big(\sum_{m=1}^{N-1}\sum_{n=m+1}^{N}\left|\Gamma_{mn}(f,x,y,z)\right|^{2}\Big)^{-1/2} \quad (6)$$

where $A(f,x,y,z)$ is the ambiguity function, defined as

$$\Gamma_{mn}(f,x,y,z) = \frac{R_m(f,x,y,z)R_n^{\mathrm{H}}(f,x,y,z)}{\left|R_m(f,x,y,z)R_n^{\mathrm{H}}(f,x,y,z)\right|} - \frac{S_m(f)S_n^{\mathrm{H}}(f)}{\left|S_m(f)S_n^{\mathrm{H}}(f)\right|}. \quad (7)$$

where N, $(.)^{\mathrm{H}}$ and $R_j(f,x,y,z)$ are respectively the number of sensors, the Hermitian operator, and the modeled signal (constructed by (4) when S is equal to one) at the j^{th} sensor at frequency f and with the hypothetical source location (x; y; z).

Also, S_j (f) is the measured signal of the j^{th} sensor at frequency f. Then, by knowing the location of the source and using the proposed algorithm described in Fig. 6, the target echo will be estimated.

The main purpose of this method is to set the null in the direction of the emitting source signal. This is done by subtracting the appropriate modeled signals of hydrophones from the associated measured signals.

The appropriate modeled signals are obtained by multiplying (4) by a phasor with an appropriate initial time, i.e., $e^{-i2\pi f t_0}\times P_{sr}$, where t_0 is the appropriate initial time. Sweeping the initial time, the appropriate initial time gives the minimum energy of the subtracted signal at the source location. Then,

TABLE 1. ***Pseudocode of the proposed source localization algorithm.***

	Algorithm **Incoherent MFP**
1:	**procedure** Localization $(c, \rho, D, f_{min}, f_{max}, x_{min}, x_{\max}, y_{\min}, y_{\max}, z_{\min}, z_{\max}, s_1, s_2, s_3, s_4, s_5)$
2:	**Initialize:** $\Gamma \leftarrow 0,\ \tilde{x} \leftarrow 0,\ \tilde{y} \leftarrow 0,\ \tilde{z} \leftarrow 0;$
3:	**for** $i = 1 \rightarrow 5$ **do**
4:	**for** $f_1 = f_{min} \rightarrow f_{max}$ **do**
5:	$S_i(f_1) \leftarrow$ Fast Fourier Transform of s_i
6:	**end for**
7:	**end for**
8:	**for** $x = x_{min} \rightarrow x_{\max}$ **do**
9:	**for** $y = y_{min} \rightarrow y_{\max}$ **do**
10:	**for** $z = z_{min} \rightarrow z_{\max}$ **do**
11:	$\xi \leftarrow 0$
12:	**for** $f = f_{min} \rightarrow f_{max}$ **do**
13:	$\beta \leftarrow 0$
14:	**for** $m = 1 \rightarrow 4$ **do**
15:	**for** $n = m+1 \rightarrow 5$ **do**
16:	Calculating the modeled signals $R_m(f,x,y,z)$ and $R_n(f,x,y,z)$;
17:	$\beta \leftarrow \beta + \left\lvert \frac{R_m(f,x,y,z)R_n^H(f,x,y,z)}{\lvert R_m(f,x,y,z)R_n^H(f,x,y,z)\rvert} - \frac{S_m(f)S_n^H(f)}{\lvert S_m(f)S_n^H(f)\rvert} \right\rvert^2$
18:	**end for**
19:	**end for**
20:	$\xi \leftarrow \xi + \beta^{-0.5}$
21:	**end for**
22:	**if** $\xi > \Gamma$ **then**
23:	$\Gamma \leftarrow \xi,\ \tilde{x} \leftarrow x,\ \tilde{y} \leftarrow y,\ \tilde{z} \leftarrow z;$
24:	**end if**
25:	**end for**
26:	**end for**
27:	**end for**
28:	$\hat{x} \leftarrow \tilde{x},\ \hat{y} \leftarrow \tilde{y},\ \hat{z} \leftarrow \tilde{z};$
29:	**return** $(\hat{x}, \hat{y}, \hat{z})$

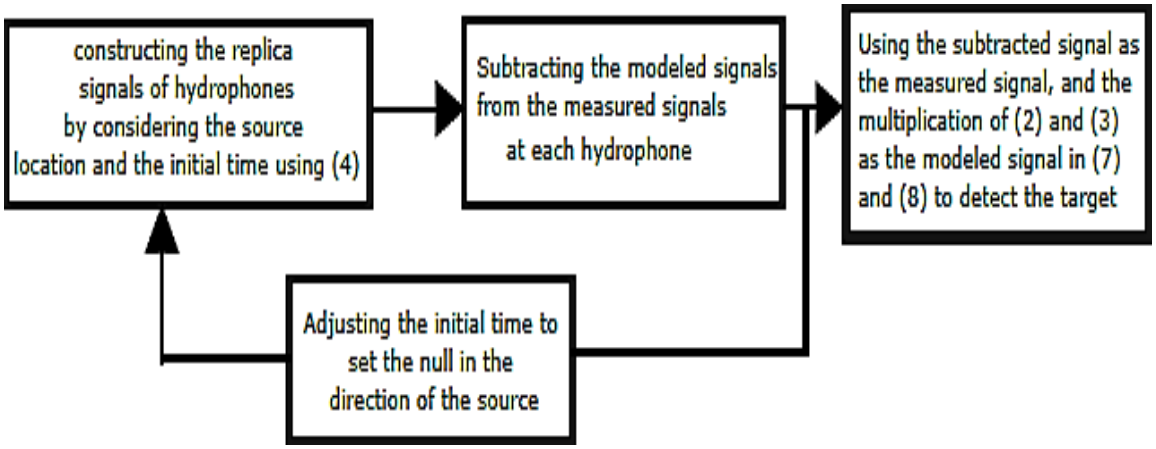

Fig. 6. The diagram of the scattering estimation algorithm.

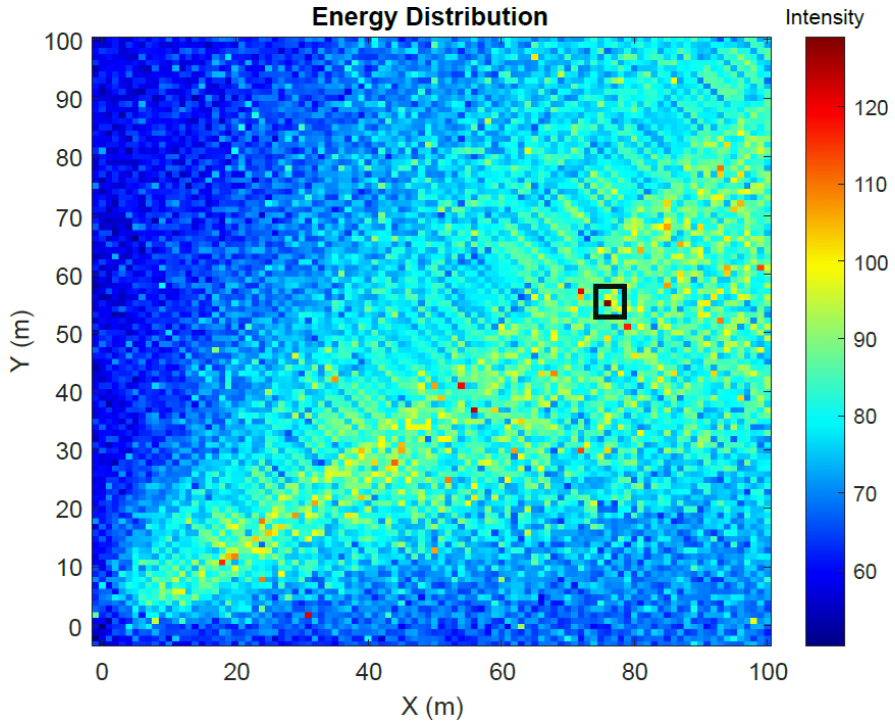

Fig. 7. Ambiguity figure of the scattering algorithm for the synthetic data in depth of 6 m.

using the resulting signals as S_j (f), $P_{st} \times P_{tr}$ as R_j in (6) and (7), the location of maximum scattering is obtained.

To evaluate the efficiency of the proposed algorithm, the simulations are carried out both using the synthetic data and real data obtained in Grand Passage.

The target is considered to be a cube with dimensions of one meter at the coordinates (x =80 m; y =50m; depth =0.6 m). It should be noted that the scattering coefficient from the target was assumed to be 0.9.

5. SIMULATION RESULTS FOR THE SYNTHETIC DATA

The environmental parameters were previously described in Section 2. The source is assumed to be located at coordinates (x =140m; y =140m; depth =0.5 m) and is represented using a propagating sinusoidal signal in a frequency band between 2000 Hz and 3000 Hz. The hydrophone array that is shown in Fig. 3, includes five elements that is lowered to the depth of 19.3 m. Also, the

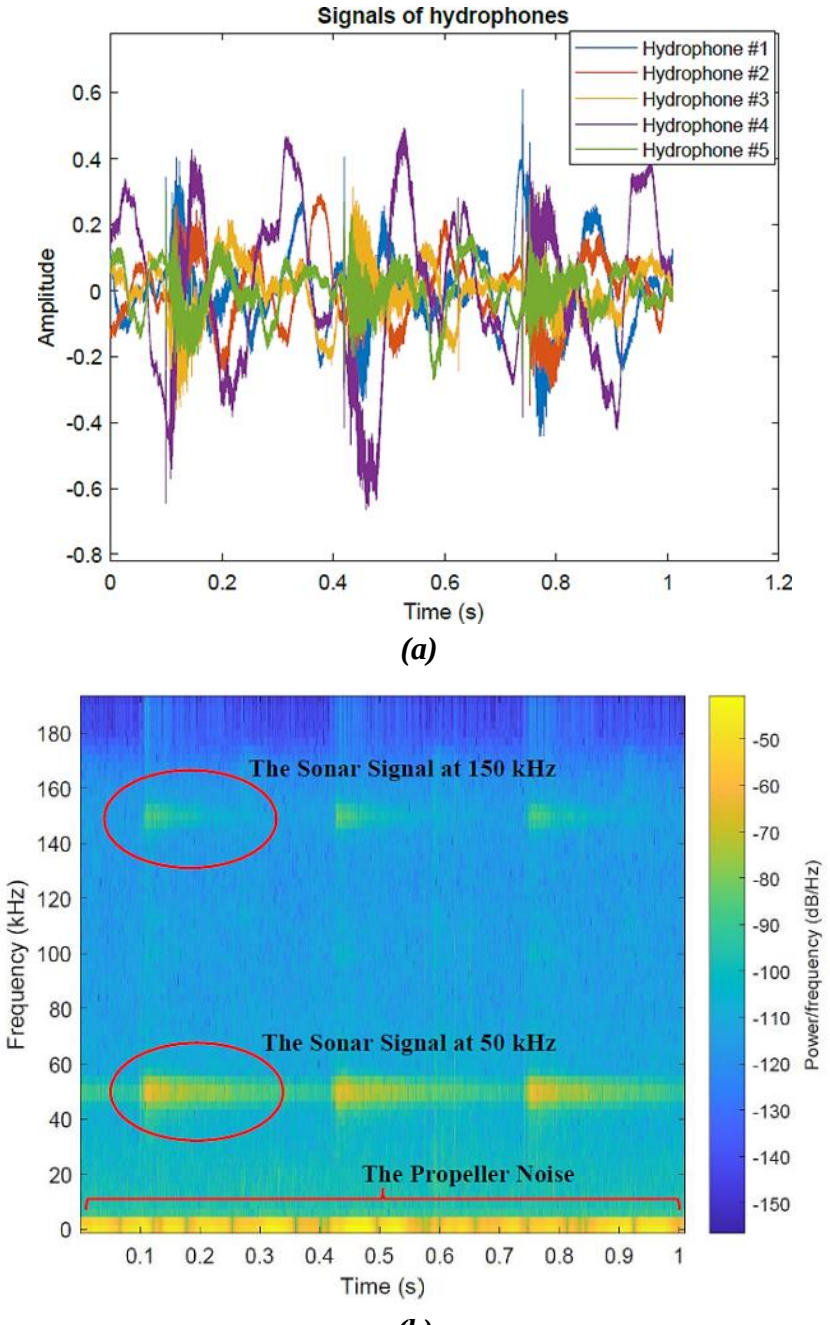

Fig. 8. (a) Propeller noise at each hydrophone in the time-domain, (b) Spectrogram of the propeller noise and sonar signal of the ship received at the 4th hydrophone.

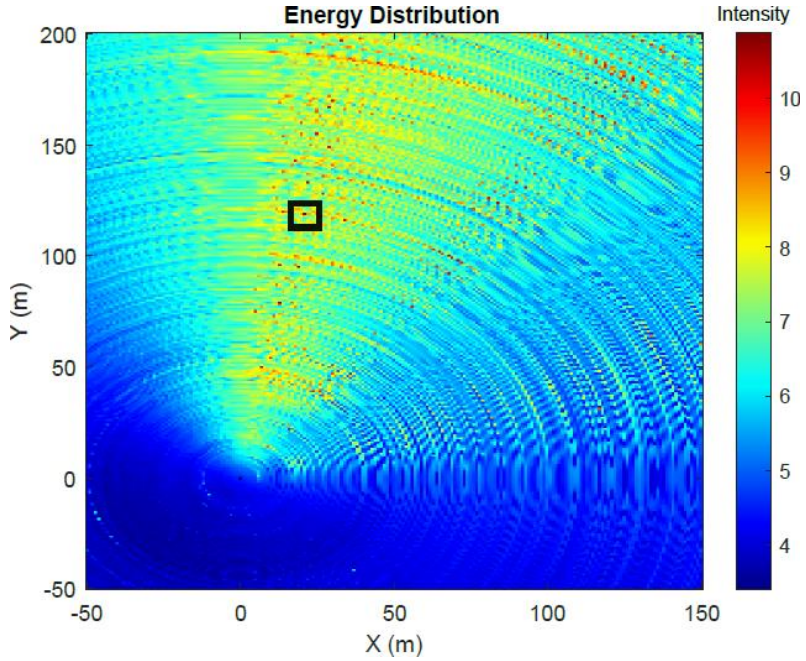

Fig. 9. Ambiguity figure for localizing the source. The estimated source location is (X =25m;Y =119m; Depth =0.6 m).

sampling frequency is 384 kHz. The high sampling frequency is chosen to acquire a broad frequency spectrum, which can also sense acoustic signatures from different marine animals.

The target is considered to be a cube with dimensions of one meter at the coordinates (x =80 m; y =50m; depth =0.6 m). It should be noted that the scattering coefficient from the target was assumed to be 0.9.

The maximum energy, in Fig. 7, shows the approximate position of the target at a coordinate of $(\hat{x}, \hat{y}) = (76\,\mathrm{m}, 55\,\mathrm{m})$ which is identified by the proposed algorithm at the depth of 0.6 m. The main reason for the difference between the main position of the target and the identified position is the intense reflections from the bottom and surface in shallow water.

6. EXPERIMENTAL RESULTS FOR THE GRAND PASSAGE DATA SET

In this section, the algorithm is tested using data acquired during the sea trial in Grand Passage.

The received signals from the hydrophones are separated using a band-pass filter in the frequency range from 2000 Hz to 3000 Hz. Then, the resulting signals are applied to the proposed algorithm, which is summarized in Table 1, to localize the boat using its propeller noise. Fig. 8 shows the signals of the hydrophones in the time-domain and frequency domain.

As can be observed in Fig. 8 (b) the boat sonar is a high-frequency signal in the 50 kHz band, as well as in the 150 kHz frequency band and can be used to calibrate the bearing of the receiver after it is deployed underwater elaborate on the importance of the work or suggest applications and extensions.

Fig. 9 shows the ambiguity function to estimating the source location. Then, according to Fig. 6, the replica signals with

the optimal initial time are made and subtracted from the measured signals to eliminate the signal effect in the direction of the source.

Finally, the remaining signal will be the results of the scattering, which, by sweeping the space, identifies the position of the strongest scatterer. According to Fig. 11, the specific area with the greatest scattering is the result of the pressure case (as shown in Fig. 2), and other scattering points exist due to the hydrophones.

To evaluate the depth of the ocean in which a target can be detected using ship noise, it is necessary to calculate the transmission loss versus the range and depth of the ocean. The transmission loss is defined by

$$\mathrm{TL}(r,z) = -20\log\left|4\pi \times (P(r,z))\right| \quad (8)$$

where $P(r,z)$ is the propagated pressure field by the ship noise. Fig. 12 presents the calculated transmission loss versus range and depth based on the following parameters. As can be observed, there is the transmission loss in the red or yellow areas due to the evanescent mode therefore, the probability of identifying the target is low in these areas.

- Depth of source, Z_s=0.6 m.
- The range interval, r = 1 to 1,000 m
- Depth of water, D=20 m.
- The thickness of the sediment layer = 20 m.
- Sound speed in sediment layer =1600 m/s.
- Average frequency = 2500 Hz.
- Number of modes=80.
- Density of the sediment layer =1500 kg/m^3.

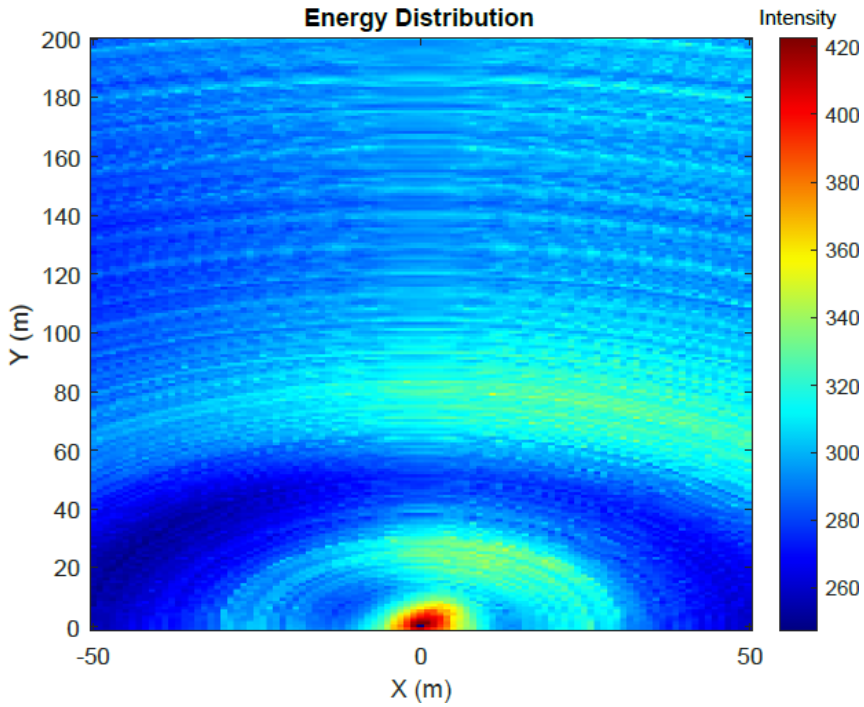

Fig. 10. Ambiguity figure for localizing the source in depth of 0.6 m after eliminating the effect of propeller noise in the direction of the source.

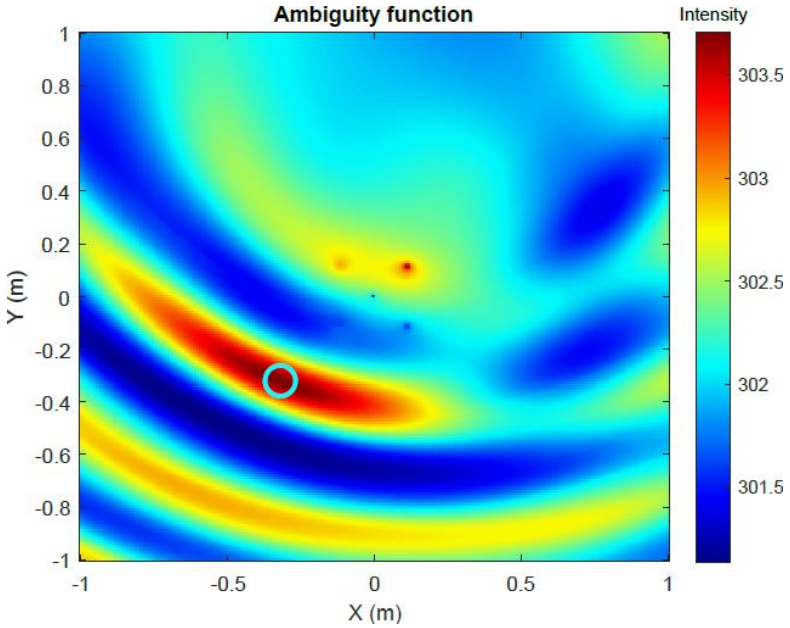

Fig. 11. Ambiguity figure for localizing the target using the scattering model in depth of 19.9 m after eliminating the effect of propeller noise in the direction of the source.

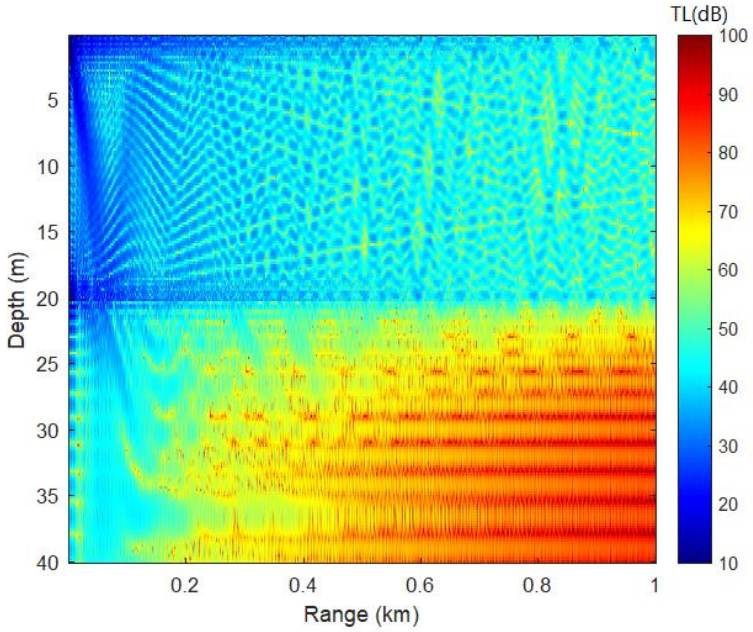

Fig. 12. Transmission loss result for the Bay of Fundy versus range and depth.

According to Fig. 12, if the target is located in the blue areas, it is more likely to be detected with high accuracy.

In this simulated model, around 40 propagating modes and 40 bottom interacting modes are used in the Legendre-Galerkin calculation [13]. Under these conditions, as shown in Fig. 12, the transmission loss is relatively low through the entire water column for ranges less than 100 meters.

7. CONCLUTION

To summarize, the normal mode approach for modeling the target echo in a bistatic geometry using the broadband ship noise is discussed. This noise is a form of signaling that can play the role of pings in active sonars. The recurrent echo was continually received by a horizontal and circular hydrophone array due to the reflection from the target. Then, the source localization was done using incoherent MFP.

Finally, using the target echo formulation, which is based on the normal modes, the target echo was detected. This idea was demonstrated using synthetic data, and it was verified using real acoustic data from the boat fishing noise in Grand Passage.

We could detect a target (pressure case) that was located near the receiver using the proposed algorithm.

Also, the Legendre-Galerkin toolbox was used for simulating the transmission loss as a function of depth and range to demonstrate which position is suitable for the echolocation of the target with respect to ship noise as an active sound source.

The results showed that this technique, which is a form of opportunistic use of ambient noise and is a relatively low-cost technique, will be practical in various fields in oceanography.

REFERENCES

[1] T. Christopher M. Verlinden; Acoustic sources of opportunity in the marine environment – applied to source localization and ocean sensing, Ph.D. dissertation, University of California, San Diego, 2017.

[2] D. P. Knobles, Maximum entropy inference of seabed attenuation parameters using ship radiated broadband noise, The Journal of the Acoustical Society of America, 2015, 138, (6), pp. 3563-3575, doi: 10.1121/1.4936907.

[3] D. Tollefsen, S. E. Dosso, and D. P. Knobles, Ship-of-opportunity noise inversions for geoacoustic profiles of a layered mud-sand seabed, IEEE Journal of Oceanic Engineering, 2020, 45, (1), pp. 189-200.

[4] M. Mirzaei Hotkani, S. A. Seyedin, Estimating the Position of Underwater Targets Based on the Emission of Noise Caused by Spinning the Propeller of Surface Vessels', 2019 Sixth Iranian Conference on Radar and Surveillance Systems, 2019, pp.1-6, doi: 10.1109/ICRSS48293.2019.9026552.

[5] M. Liefvendahl, A. Feymark and R. Bensow, Methodology for noise source modelling and its application to Baltic Sea shipping, the BONUS SHEBA project. 2015.

[6] M. Mirzaei Hotkani, S. A. Seyedin, and J. F. Bousquet, Underwater Object Localization using the Spinning Propeller Noise of Ships Based on the Wittekind Model, International Journal of Engineering and Advanced Technology, 2020, 9, (3), pp. 2736-2741, doi: 10.35940/ijeat.C6054.029320.

[7] M. F. McKenna, D. Ross, S. M. Wiggins, and J. A. Hildebrand, Underwater radiated noise from modern commercial ships, *J. Acoust. Soc. Am.*, 2012.

[8] F. B. Jensen, W. A. Kuperman, M. B. Porter, and H. Schmidt, Computational ocean acoustics, Springer Science & Business Media, 2011.

[9] H. P. Bucker, and H. E. Morris, Normal-mode reverberation in channels or ducts," J. Acoust. Soc. Am. 44, 827-828. 1968.

[10] R. H. Zhang, and G. L. Jin, Normal-mode theory of the average reverberation intensity in shallow water, J. Sound Vib. 119, 215-223. 1987.

[11] D. D. Ellis, J. Yang, J. R. Preston, and S. Pecknold, A normal mode reverberation and target echo model to interpret towed array data in the target and reverberation experiments, IEEE Journal of Oceanic Engineering, pp. 344-361, 2017.

[12] Tran, P. N. and Trinh, K. D.: 'Adaptive Matched Field Processing for Source Localization Using Improved Diagonal Loading Algorithm', Acoustics Australia, 2017, pp. 325-330. doi: /10.1007/s40857-017-0089-4.

[13] R. B. Evans, "The rate of convergence and error distribution of Galerkin approximations to eigenvalues in underwater acoustics," *J. Acoust. Soc. Am.*, 2013.

[14] M. Gorji, H. Ghassemi, and J. Mohamadi, "Calculation of sound pressure level of marine propeller in low frequency," *J. Low Freq. Noise Vib. Act. Control*, 2018.